iScience

CellPress
OPEN ACCESS

Article

Functions of MnO_x in NaCl Aqueous Solution for Artificial Photosynthesis

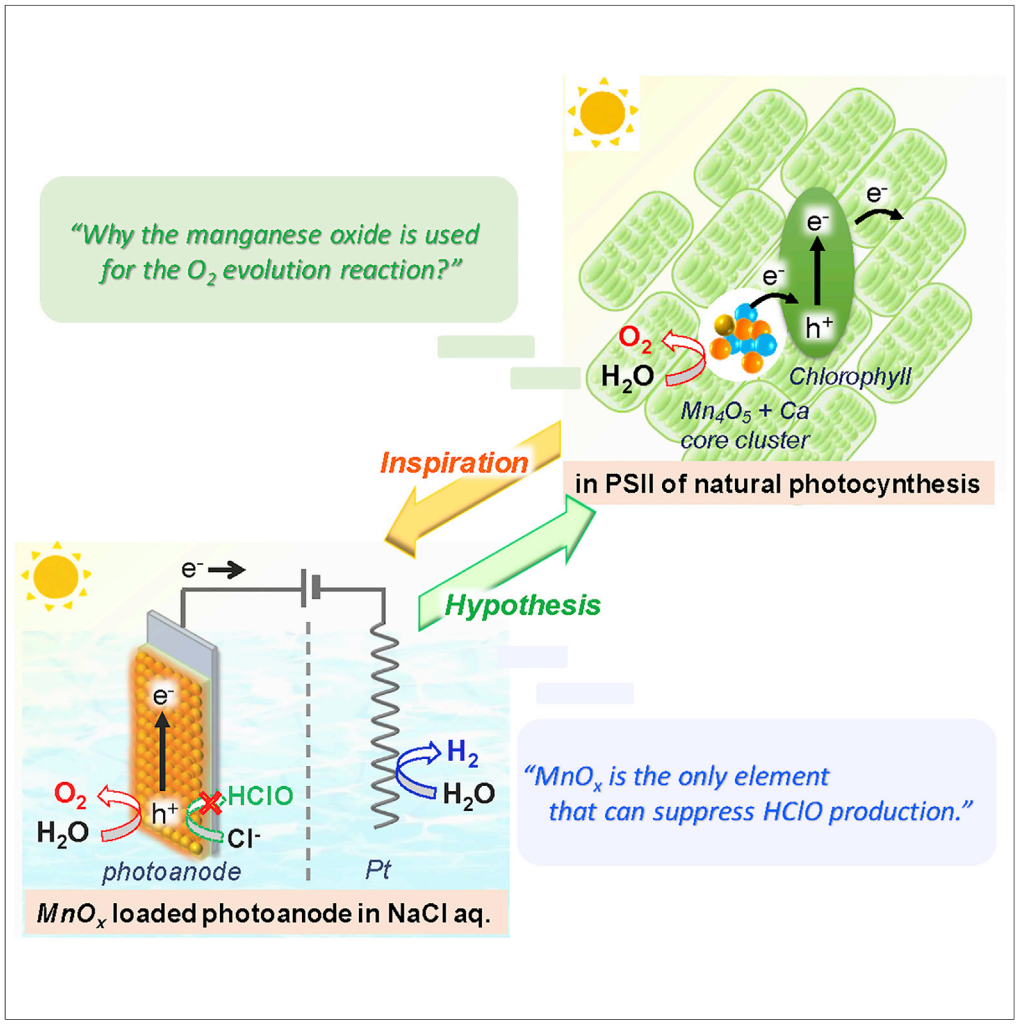

Sayuri Okunaka, Yugo Miseki, Kazuhiro Sayama

k.sayama@aist.go.jp

HIGHLIGHTS

Selectivity of O_2/HClO production in NaCl aq. sol. on photoanodes was investigated

MnO_x modification promoted O_2 evolution specifically without HClO production

The results are useful for practical application of artificial photosynthesis

A hypothesis about the evolution in natural photosynthesis was proposed

Okunaka et al., iScience *23*, 101540
October 23, 2020
https://doi.org/10.1016/j.isci.2020.101540

iScience

CellPress
OPEN ACCESS

Article

Functions of MnO_x in NaCl Aqueous Solution for Artificial Photosynthesis

Sayuri Okunaka,[1] Yugo Miseki,[1] and Kazuhiro Sayama[1,2,*]

SUMMARY

Photoelectrochemical water splitting has been intensively investigated as artificial photosynthesis technology to convert solar energy into chemical energy. The use of seawater and salted water has advantages for minimum environmental burden; however, the oxidation of Cl^- ion to hypochlorous acid (HClO), which has toxicity and heavy corrosiveness, should occur at the anode, along with the oxygen evolution. Here, O_2 and HClO production in aqueous solution containing Cl^- on photoanodes modified with various metal oxides was investigated. The modification of MnO_x resulted in the promotion of the O_2 evolution reaction (OER) specifically without HClO production over a wide range of conditions. The results will contribute not only to the practical application of artificial photosynthesis using salted water but also to the elucidation of substantial function of manganese as the element for OER center in natural photosynthesis.

INTRODUCTION

Various photoanodes composed of oxide semiconductors on conducting glass substrate have been widely studied for artificial photosynthesis technology with water oxidation into O_2 under simulated solar light and low applied bias in aqueous electrolyte solution (Fujishima and Honda, 1972; Hisatomi et al., 2014; Kang et al., 2015; Sivula and van de Krol, 2016; Roger et al., 2017), whereby the efficiency was determined to be improved by loading with metal oxides (MO_x) such as FeO_x, NiO_x, and CoO_x (Zhong et al., 2015; Chemelewski et al., 2014). The ability of O_2 evolution reaction (OER) of MO_x has been further improved by modification with phosphate, borate, and carbonate ions (Kim and Choi, 2014; Bediako et al., 2012; Li et al., 2016). Moreover, the use of seawater and salted water for electrolyte solution has been investigated because of some significant advantages to minimize the environmental burden and provide cost reduction on electrochemical systems using photoanodes (Desilvestro and Gräetzel, 1987; Luo et al., 2011; Barczuk et al., 2013; Fukuzumi et al., 2017; Iguchi et al., 2018) as well as metal anodes (Bennet., 1980; El-Moneim et al., 2009; Vos et al., 2018; Ibrahim and Canan, 2015; Gidon et al., 2018). However, in seawater containing Cl^- anions, hypochlorous acid (HClO, neutral form of Cl_2) production reaction (abbreviated as CPR) by Cl^- oxidation proceeds concurrently with the OER by water oxidation (Figure 1). Although HClO is a valuable chemical for disinfection and bleaching to some extent (Sayama, 2018), control of the selectivity and the suppression of CPR on photoanodes are important requirements for H_2 production in large-scale water-splitting systems because of the toxicity and corrosiveness of HClO (Fujimura et al., 1999). The CPR via 2-electron reaction proceeds easily compared with the OER via 4-electron reaction, whereas the OER is more preferable to the CPR with respect to the redox potential ($HClO/Cl^-$ = ca. +1.28 V and O_2/H_2O = +0.83 V versus SHE, pH = 7). There have been some reports that the CPR on metal anodes is effectively suppressed by the use of cation-exchange membranes or entirely coating the anode with MnO_x as Cl^--impermeable layers (El-Moneim et al., 2009; Vos et al., 2018; Balaji et al., 2009), and by buffered conditions to maintain an alkaline pH (Dionigi et al., 2016). However, it is more difficult to suppress the CPR in unbuffered NaCl solution because the anode is subjected to partially acidic conditions. Here, we systematically investigated the effect of loading various simple metal oxide species (MO_x), including precious metals, on the selectivity toward $HClO/O_2$ production from unbuffered NaCl aqueous solution over a $BiVO_4$ photoanode, which is one of the most popular visible-light responsible photoanodes for efficient water splitting (Hong et al., 2011; Saito et al., 2012; Fuku et al., 2017), and found that MnO_x loading could specifically suppress the CPR on the photoanode under a wide range of conditions. Finally, we could advocate a new hypothesis why manganese is selected as the element for OER center of natural photosynthesis (Barber., 1998; Yano et al., 2006; Umena et al., 2011). (Figure 1)

[1]Global Zero Emission Research Center (GZR), National Institute of Advanced Industrial Science and Technology (AIST), 1-1-1 Higashi, Tsukuba, Ibaraki. 305-8565, Japan

[2]Lead Contact

*Correspondence: k.sayama@aist.go.jp

https://doi.org/10.1016/j.isci.2020.101540

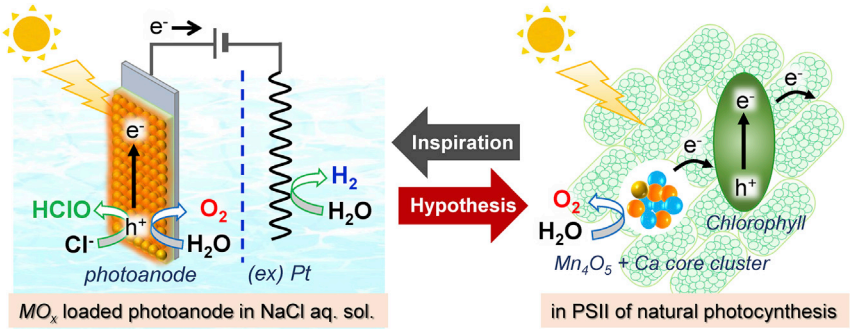

Figure 1. Reaction Images of the Artificial/Natural Photosynthesis Systems

Reaction images of the artificial photosynthesis system using MO_x-loaded $BiVO_4/WO_3$/FTO photoanode (left) and Mn_4O_5 + Ca core cluster for OER and chlorophyll in PSII of natural photosynthesis (right).

RESULTS AND DISCUSSION

Properties of $MO_x/BiVO_4/WO_3$/FTO under Simulated Solar Light

A multilayer photoanode of $BiVO_4/WO_3$/FTO (FTO = F-doped SnO_2 conducting glass), which has excellent performance for water splitting into H_2 and O_2 under low applied bias (Hong et al., 2011; Saito et al., 2012; Fuku et al., 2017), was used in this work. Figure 2A shows the faradaic efficiencies (FE) for O_2 and HClO generation (FE(O_2) and FE(HClO)) from aqueous NaCl solution on a $BiVO_4/WO_3$/FTO photoanode loaded with/without MO_x under simulated solar light (AM 1.5, 1 SUN). The potential required for the photo-electrolysis for steady current (2 mA) using these photoelectrodes was listed in Table S1. The bare photoanode produced both HClO and O_2, and other oxidative by-products (Cl_2, $HClO_2$, $HClO_3$ etc.) were not generated, as we recently reported (Iguchi et al., 2018). For the all photoanodes, the sum of FE for the oxidative products (O_2 and HClO) became around 100% considering the measurement error (ca. 15%), which suggested the main products were O_2 and HClO. O_2 production with a high FE(O_2) of >90% was observed on the $MnO_x/BiVO_4/WO_3$/FTO photoanode, and no significant amount of HClO was detected with MnO_x loading. FE(HClO) with a CoO_x-loaded photoanode was increased to ca. 88%. The dependence of FE(HClO) on the concentration of the Mn precursor solution and the concentration or pH of aqueous NaCl electrolyte solution were also investigated (Figures 2B–2D), and the CPR was effectively suppressed when the Mn precursor concentration was ≧0.01 M, the NaCl concentration was between 0.05 M–2 M, or the pH was between 3 and 9, respectively. Figure S1A shows current-potential (*I-V*) curves for the $MnO_x/BiVO_4/WO_3$/FTO photoanodes under simulated solar light though a light chopper. The photocurrent could be observed on the photoanodes with or without MnO_x at much less than +0.88 V versus SHE, pH = 7. The optimum preparation temperature for MnO_x loading was 400°C for the best photocurrent among all MnO_x-loaded photoanodes (Figure S1B). The photocurrent could be kept at almost 80% after MnO_x loading compared with that of the bare photoanode, because the color of the photoanode became brown and the photoabsorption might be inhibited by MnO_x loading (Figure S1C). Another possibility of decreased photocurrent could be considered to be producing some doped layers to accelerate charge recombination at the interface of $MnO_x/BiVO_4$ during the calcination process. We also examined the photoelectrochemical CPR in artificial seawater rather than in pure NaCl solution (Figure S2). The behavior of HClO selectivity in artificial seawater was very similar to that in pure NaCl solution (Figure 2A), and only the MnO_x-loaded photoanode suppressed the CPR efficiently. The results suggest no significant effect of various anions and cations contained in the artificial seawater, such as SO_4^{2-} and Mg^{2+}, on the selectivity due to the low concentrations of these ions compared with Na^+ and Cl^- (Desilvestro and Gräetzel, 1987; Luo et al., 2011; Barczuk et al., 2013; Fukuzumi et al., 2017; Iguchi et al., 2018). It was also confirmed that H_2 was produced on a Pt cathode in artificial seawater with a high FE(H_2) (ca. 100%).

Characterizations of $MO_x/BiVO_4/WO_3$/FTO

The amounts of MO_x loading on the $BiVO_4/WO_3$/FTO photoanodes calculated from X-ray fluorescence (XRF) measurements are summarized in Table S2. The amount of MnO_x was 0.02 μmol/cm^2, and those of other MO_x were in a similar range between 0.01 and 0.024 μmol/cm^2. Surface scanning electron microscopic (SEM) observations of bare $BiVO_4/WO_3$/FTO (Figure 3A-(i)) confirmed a nanostructure with particle networks that consist of primary particles with diameters of ca. 100 nm. In contrast, the edge of the particles on the photoelectrode was not clear for MnO_x(0.1 M)/$BiVO_4/WO_3$/FTO (Figure 3A-(ii)), which suggests the loaded MnO_x covered the entire

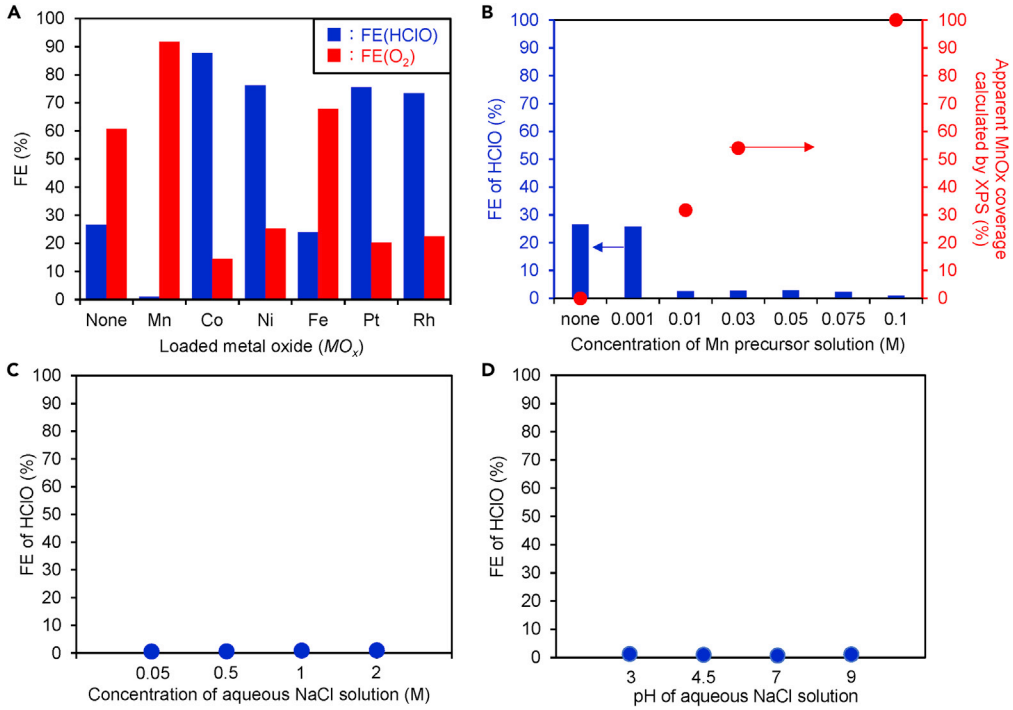

Figure 2. Photoelectrochemical Properties of MO_x-Loaded Photoanodes

(A) FEs for O_2 and HClO generation on photoanodes (MOx/$BiVO_4$/WO_3/FTO) modified with and without various metal oxides. The concentrations of loaded metal precursor solution were 0.1 M for Mn, Co, Ni, and Fe and 0.03 M for Rh and Pt. The calcination temperature for loading was 400°C, at an electric charge of 2 C (1,000 s and a steady photocurrent of 2 mA) in a 0.5 M NaCl aqueous electrolyte (35 mL) under simulated solar light (AM-1.5, 1 SUN).

(B) FE (HClO) and apparent MnO_x-coverage calculated from XPS results for bare $BiVO_4$/WO_3/FTO and MnO_x/$BiVO_4$/WO_3/FTO photoanodes, which were prepared by coating the manganese precursor solution with different concentrations (0.001–0.1 M) to change the MnO_x loading amount.

(C) FE (HClO) on MnO_x (0.1 M)/$BiVO_4$/WO_3/FTO in aqueous NaCl solution with various concentrations (0.05-2 M).

(D) FE (HClO) on MnO_x (0.1 M)/$BiVO_4$/WO_3/FTO anode in 0.5 M aqueous NaCl solution with various pH (pH 3–9).

surface of the photoanode. Transmission electron microscopic-energy dispersive X-ray spectroscopic (TEM-EDX) cross-sectional images of the photoanode loaded with MnO_x (0.1 M, Figure 3B) showed that a thin layer (ca. 10–30 nm thick) of MnO_x was present over the surface of the $BiVO_4$/WO_3/FTO photoanode. No electron diffraction pattern was obtained at the MnO_x part, which indicates that MnO_x was not crystalline. The apparent surface coverage of MO_x layers calculated from the peak area of X-ray photoelectron spectroscopy (XPS; Figure 3C) measurements are summarized in Table S3. In the case of the MnO_x (0.1 M)-coated sample, the peaks attributed to Bi, V, W, and Sn of the photoanode were not observed, whereas the peak attributed to Mn $2p_3$ was clear, which suggested the surface coverage of MnO_x was almost 100%. In contrast, for the MnO_x (0.03 M)-coated sample, the peaks attributed to Mn $2p_3$ decreased and peaks attributed to V $2p_3$, Bi $4f_{7/2}$, W 4f, and Sn 3d were observed, which indicates that MnO_x(0.03 M) was not completely covering the photoanode surface, unlike that prepared with 0.1 M precursor solution. The dependence of the apparent surface coverage of MnOx on the concentration of manganese precursor solution is shown by the right-hand axis in Figure 2B. The coverage of MnO_x decreased on decreasing the concentration of the manganese precursor solution. Although the apparent surface coverage of MnO_x (0.01 M)-loaded $BiVO_4$/WO_3/FTO photoanode was only 30%, the selectivity toward the CPR was very low. Therefore, it is concluded that entire coverage of MnO_x on the $BiVO_4$/WO_3/FTO surface was not necessary to suppress the CPR. The results indicate that the selectivity toward HClO/O_2 production could be controlled by this simple coating method using metal precursor solutions, and the CPR could be suppressed in aqueous solution containing Cl^- ions with a photoanode surface partially loaded with MnO_x.

Properties of MO_x/FTO under Dark Conditions

The electrochemical properties of the simple structured-MO_x/FTO anodes without semiconductor layers were also evaluated under dark conditions (Figure S3). We checked the product amount of HClO/O_2

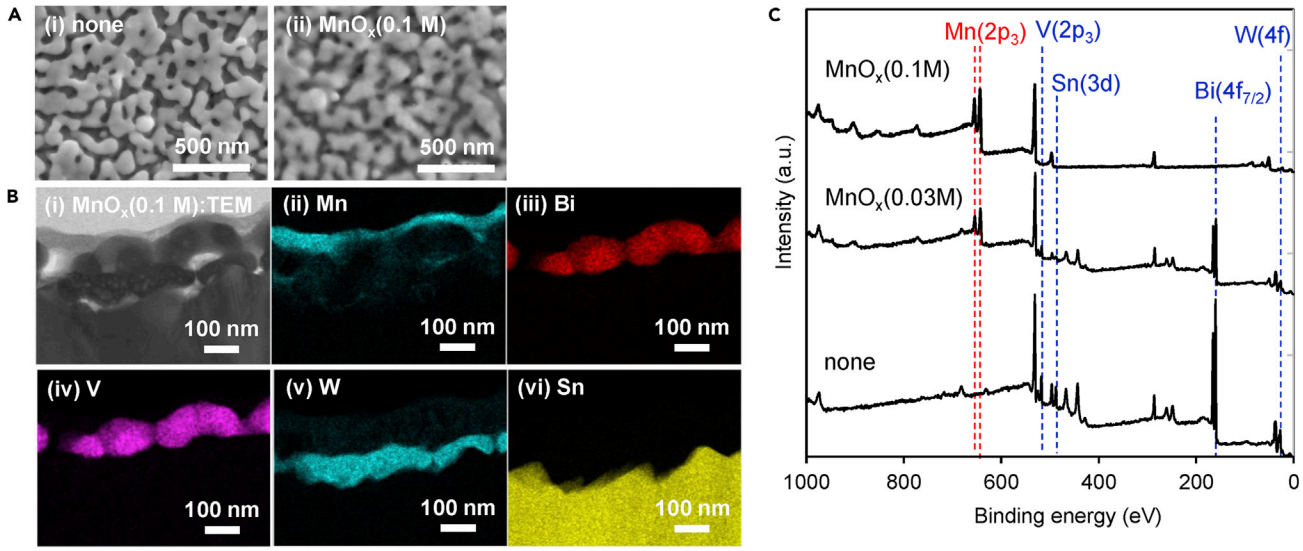

Figure 3. Characterization of $BiVO_4/WO_3$/FTO Photoanodes with and without Loading MnO_x

(A–C) (A) Surface SEM images, (B) cross-sectional TEM-EDX images, and (C) XPS spectra of $BiVO_4/WO_3$/FTO photoanodes with and without MnO_x. (A (ii) and B) The concentration of the MnO_x precursor solution was 0.1 M. (B) (i) TEM image and (ii-vi) EDX mapping images for each element.

and calculated the values of FE(HClO), FE(O_2) on bare FTO, and *MOx*/FTO, confirming that the sum of the FE(HClO) and FE(O_2) became almost 100% within variation of measurement errors in each electrode. FE(HClO) for various MO_x/FTO anodes (Figure S3A) had a similar tendency to that for the $MO_x/BiVO_4/WO_3$/FTO photoanodes (Figure 2A). It was also confirmed that MnO_x loading of the anodes effectively suppressed the CPR in aqueous NaCl solution under a wide range of conditions, regardless of the Mn precursor solution concentration (0.01–0.1 M), the NaCl concentration (0.005–2 M), pH (3–9), applied bias (1.5–1.8 V versus SHE, pH = 7), the valence or structure of MnO_x (amorphous, Mn_2O_3 and Mn_3O_4), preparation methods of MnO_x such as calcination temperature (300–550°C), and the kinds of manganese salt dissolving the precursor solution, as shown in Figures S3B–S3I. SEM images, MnO_x coverages, and FE(HClO) of MnO_x/FTO anodes are shown in Figure S4. In the case of the MnO_x (0.03 M)/FTO with very low FE(HClO), SEM observations indicated that MnO_x did not entirely coat the surface of FTO, and the apparent coverage of MnO_x (0.03 M) calculated from the XPS spectrum was only 65%. It is suggested that complete coating of MnO_x on FTO anodes was not needed to suppress the CPR, as well as photoanodes.

Mechanism of Selective O_2 Production on MnO_x-Loaded Photoanode

There are two possibilities why the MnO_x loaded on the photoanodes or anodes could suppress the CPR; direct O_2 production on MnO_x and indirect O_2 production through the decomposition of HClO as an intermediate. The HClO initially added to the NaCl aqueous solution was not decomposed on a MnO_x/FTO anode under dark conditions (Figure S5). This suggests that indirect O_2 production on MnO_x/FTO by HClO decomposition on the MnO_x surface can be denied and that O_2 was directly produced on MnO_x/FTO in NaCl aqueous solution.

In the case of noble metal anodes such as IrO_2, selective OER from an aqueous solution containing Cl^- ions can be realized by coating an MnO_x layer on the entire surface of the anode (Bennet, 1980; El-Moneim et al., 2009; Vos et al., 2018; Ibrahim and Canan, 2015; Gidon et al., 2018). In the field of water electrolysis, this selective OER has been explained by a "Cl^--impermeable mechanism," where Cl^- ions cannot reach the surface of the noble metal through the MnO_x layer, rather than by a "catalytic mechanism" where MnO_x itself functions as an electrocatalyst for O_2 production (Vos et al., 2018). In this Cl^--impermeable mechanism, the MnO_x layer must completely cover the entire surface of the noble metal, and no oxidation reaction should occur on the MnO_x but rather on the noble metal catalyst, which indicates that the reaction sites are completely different with each mechanism. However, in this study, much data that cannot be explained by the Cl^--impermeable mechanism was obtained. First, current-voltage (*I-V*) curves for the MnO_x/FTO anode showed that the onset potential was significantly shifted to lower potential compared with that for bare FTO (Figures 4A and 4B). Second, complete coating of MnO_x on FTO anode was not necessary

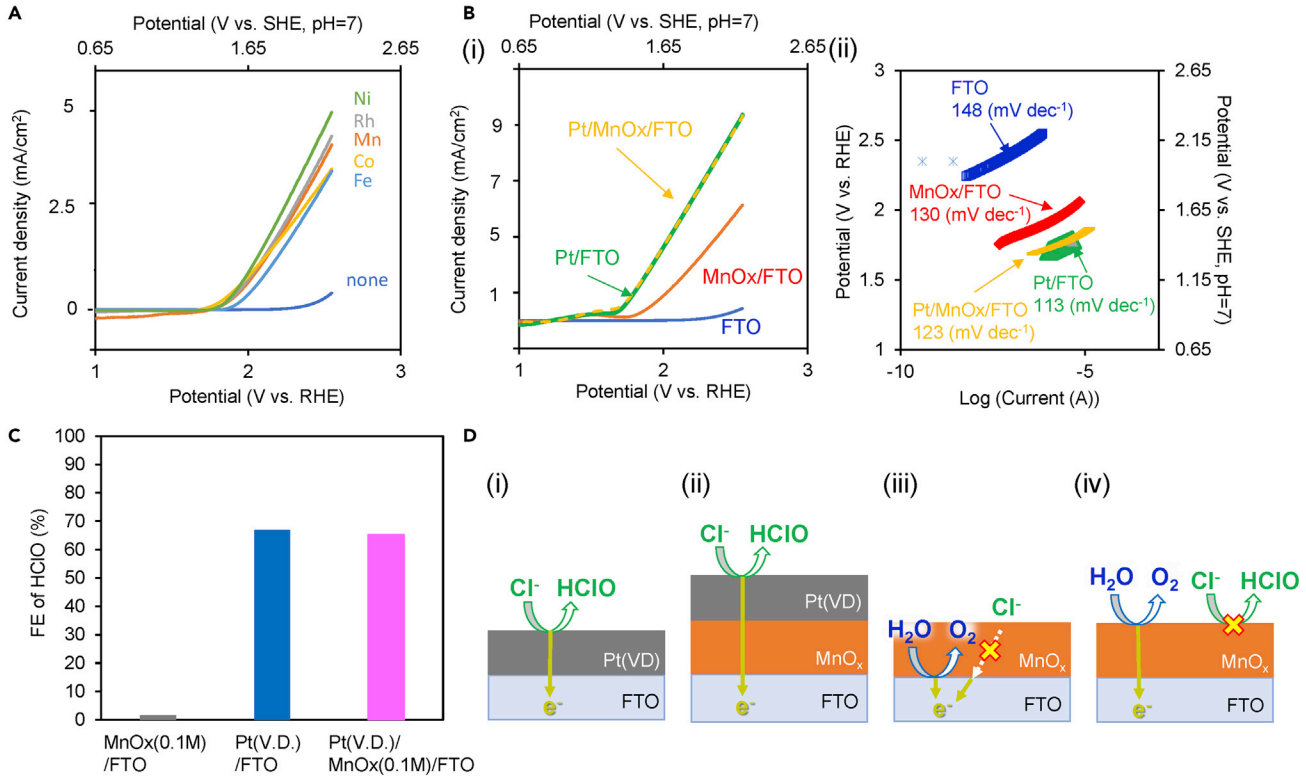

Figure 4. Evaluation of Electrochemical Properties and Schematic Diagrams on O_2/HClO Production on MO_x/FTO Anodes

(A) *I-V* characteristics for bare FTO and various MO_x (0.1 M)/FTO anodes measured in 0.5 M NaCl aqueous solution (sweeping in the cathodic direction).

(B) (i) *I-V* characteristics and (ii) Tafel plots for various anodes (FTO, MnO_x (0.1 M)/FTO, Pt(VD)/FTO, and Pt(VD)/MnO_x (0.1 M)/FTO) measured in 0.5 M NaCl aqueous solution. The Pt (VD) layer was prepared using the vapor deposition method.

(C) FE (HClO) for various anodes at an electric charge of 2 C (1,000 s at a steady current of 2 mA) in a 0.5 M aqueous NaCl solution.

(D) Schematic diagrams of (i) Pt (VD)/FTO and (ii) Pt (VD)/MnO_x (0.1 M)/FTO anodes. (iii) Cl^--impermeable mechanism and (iv) catalytic mechanism for MnO_x (0.1 M)/FTO anodes.

to suppress the CPR (Figures S3B and S4). Third, it was confirmed whether or not the oxidation reaction occurred on MnO_x (Figures 4C and 4D). A thick MnO_x (0.1 M) layer that covered the entire FTO surface was prepared, and then it was coated with Pt by vapor deposition method (Pt (VD)/MnO_x/FTO). The *I-V* properties and Tafel slope were improved by Pt (VD) loading (Figure 4B-(ii)). The FE (HClO) on the Pt (VD)/MnO_x/FTO anode (65.2%) was almost same as that on the Pt (VD)/FTO anode (66.9%) and was completely different from that on MnO_x/FTO (<1.6%), as shown in Figure 4C, which indicates that the selectivity and *I-V* properties could be controlled by modification of the top surface. These results suggest that the oxidation reaction occurred on the top surface of MnO_x on the MnO_x (0.1 M)/FTO anode, and not on the surface of FTO (Figure 4D). Furthermore, the Cl^- adsorption characteristics of MO_x were compared using XPS, and Cl^- ions were found not to be adsorbed by CoO_x, FeO_x, NiO_x, or MnO_x (Table S4, Cl coverage <1%). Therefore, it was difficult to explain MnO_x peculiarity by the difference of the adsorption characteristics of Cl^-. From all these results, we can conclude that the mechanism for the selectivity toward the OER/CPR on MnO_x/FTO from an aqueous solution containing Cl^- ions can be explained not by the Cl^--impermeable mechanism but rather by the catalytic mechanism (Figure 4D-(iii and iv)).

The special OER selectivity on the MnO_x catalyst-loaded anodes might be explained by the difference or the ratio of the overpotential with the OER and CPR reactions in each electrolyte solution. The potentials required for steady current electrolysis on various MO_x/FTO were listed in Table S5. The behaviors of potential on each anode were similar in NaCl and NaH_2PO_4 aqueous solutions except for unstable anodes; the precious metals showed the lowest potential level, and CoO_x, FeO_x, NiO_x, and MnO_x showed the second lowest level. On the other hand, the evaluation of each specific overpotential in NaCl aqueous solution is difficult because both the OER and CPR occur. It should be emphasized again that the FE (HClO) was very low even when MnO_x was not fully coated on FTO; therefore, it is surmised that the overpotential for the

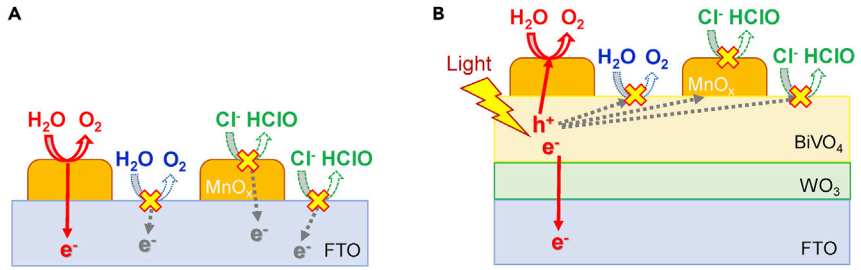

Figure 5. Schematic Diagrams on O_2/HClO Production over Partially Loaded MnO_x Catalyst

(A and B) The OER and CPR on (A) FTO anode and (B) $BiVO_4/WO_3$/FTO photoanode partially loaded with MnO_x catalyst. The selectivity is controlled by the relative relationship of the overpotentials for each reaction. The overpotential for the OER on MnO_x might be much lower than those of other reactions such as the CPR on MnO_x, and the OER and CPR on $BiVO_4$.

OER on MnO_x was much lower than those of the other reactions such as the CPR on MnO_x, and the OER and CPR on FTO relatively in NaCl solution (Figure 5A). As for the photoanode reactions using $MO_x/BiVO_4/WO_3$/FTO, the specificity of MnO_x could not be explained by the decomposition of HClO produced into O_2 by UV light excitation from solar light as reported (Fukuzumi et al., 2017), because the results in Figure 2A were compared under the same irradiation conditions. It was confirmed that the HClO selectivity was very low, even when the apparent coverage of MnO_x was only 30%, as shown in Figure 2B. Considering the analogy with the results for the MnO_x/FTO anode, the Cl^--impermeable mechanism for MnO_x loaded on a photoanode can also be excluded. The turnover number (ca. 154) of e^- to Mn on the MnO_x-loaded photoanode was much more than 1. Therefore, it is reasonable to explain the results by the catalytic mechanism, where photoexcited h^+ on $BiVO_4$ immediately moves to MnO_x and the preferential oxidation of water on the MnO_x surface into O_2 occurs without the CPR (Figure 5B). It should be noted that various MnO_x catalysts such as amorphous Mn_2O_3, Mn_3O_4, and Ca-MnO_x could suppress the CPR (Figure S3G), which indicates that manganese oxides themselves may have specificity with a large overpotential ratio for the CPR to the OER in NaCl solution. This catalytic mechanism of MnO_x is generally that for the OER on Mn_4O_5 core cluster with Ca in the photosystem II (PSII) of natural photosynthesis (Suga et al., 2017; Zhang et al., 2018; Zaharueva et al., 2011; Najafpour et al., 2010); therefore, it can also be a common mechanism in the fields of electrolysis and artificial photosynthesis using photoanodes. Currently, the intrinsic reason for the specific dependence of the overpotentials on these elements including manganese is not clear, and the comparison of energy barriers of transition state between CPR and OER on a certain model structure of each MO_x through computational chemistry is under investigation.

Evolutional Hypothesis for the Mn_4O_5 Core of Natural Photosynthesis

Natural OER metal centers of cyanobacteria, algae, or plants containing elements other than Mn have not been found to date. Mn has many advantages such as a low overpotential for OER and earth-abundant transition metal element with various valence states (Zhang et al., 2018; Armstrong., 2008; Sauer and Yachandra, 2002; Raveau and Seikh, 2012; Bryan et al., 2016). On the other hand, some metal oxides such as Fe, Ni, and Co also basically satisfy all these requirements (Zaharueva et al., 2011; Raveau and Shiek, 2012; Bryan et al., 2016). Therefore, there is no hypothesis to explain why Fe, Ni, or Co is not used as the OER center in PSII so far. Based on our specific results that MnO_x catalyzes the OER selectively from NaCl aqueous solution under a wide range of conditions, even at low pH and low Cl^- concentration compared with those for natural photosynthesis *in vivo* (ca. 100 mM of Cl^- in chloroplasts) (Robinson and Downton, 1984; Baranov and Haddy, 2017; Jagendorf and Uribe, 1966; Beebo et al., 2013), it is possible to advocate a new hypothesis as to why MnO_x is selected as the OER center of PSII that appeared on the ancient earth. It is because HClO is significantly toxic to organisms, and Mn is the only element that can produce only O_2 without the generation of HClO in aqueous solution containing Cl^- ions under various conditions *in vivo*. Considering that HClO has extremely strong bactericidal properties compared with H_2O_2 (McKenna and Davies, 1988), and that it should be necessary to avoid the generation of even a small amount of HClO in *vivo*, the specialty of natural Mn_4O_5 can be comprehensively explained by the results of this study.

Limitation of the Study

We investigated the O_2/HClO production in aqueous solution containing Cl^- on $BiVO_4/WO_3$/FTO photoanodes and FTO anodes modified with various MO_x. It is emphasized that the modification of partially

loaded MnO_x resulted in specifically catalyzing the OER without HClO production over a wide range of conditions. These results will not only provide some insight into the practical application of artificial photosynthesis technologies using salted water and solar energy but also facilitate the elucidation of the function of Mn_4O_5 core cluster with Ca in natural photosynthesis. Considering our results, one hypothesis about the evolutional process of Mn_4O_5 core cluster in natural PSII can be proposed; HClO is toxic to bacteria, so that manganese element might be selected by nature due to the unique catalysis on MnO_x, where HClO production is fully suppressed. Complete elucidation of evolutional hypothesis is difficult generally; however, our hypothesis will be elucidated by various ways. For example, we have some plans about the investigation on the effect of coordination of organic compounds with carboxyl and amino groups, mimicking the atmosphere in the protein of PSII, on various nano-size MO_x and multinuclear metal complexes as electrocatalysts systematically, as well as investigation through computational chemistry in the future.

Resource Availability

Lead Contact

Further information and requests for resources should be directed to the Lead Contact, Kazuhiro Sayama (k.sayama@aist.go.jp).

Materials Availability

This study did not generate new unique reagents.

Data and Code Availability

This study did not generate/analyze datasets/code.

METHODS

All methods can be found in the accompanying Transparent Methods supplemental file.

SUPPLEMENTAL INFORMATION

Supplemental Information can be found online at https://doi.org/10.1016/j.isci.2020.101540.

ACKNOWLEDGMENTS

This work was partially supported by Japan Society for the Promotion of Science KAKENHI Grant Number JP17H06436 in Scientific Research on Innovative Areas "Innovation for Light-Energy Conversion (I^4LEC)."

AUTHOR CONTRIBUTIONS

S.O. and K.S. designed the experiments. S.O. performed all sample preparation, characterization, and (photo)electrochemical property experiments. All authors discussed the results and commented on the manuscript.

DECLARATION OF INTERESTS

The authors declare no competing interests.

Received: April 28, 2020
Revised: June 4, 2020
Accepted: September 2, 2020
Published: October 8, 2020

REFERENCES

Armstrong, F.-A. (2008). Why did Nature chosen manganese to make oxygen? Phil. Trans. R. Soc. B *363*, 1263–1270.

Balaji, R., Kannan, B.S., Lakshmi, J., Senthil, N., Vasudevan, S., Sozhan, G., Shukla, A.K., and Ravichandran, S. (2009). An alternative approach to selective sea water oxidation for hydrogen production. Electrochem. Commun. *11*, 1700–1702.

Baranov, S., and Haddy, A. (2017). An enzyme kinetics study of the pH dependence of chloride activation of oxygen evolution in photosystem II. Photosyn. Res. *131*, 317–332.

Barber, J. (1998). Photosystem two. Biochem. Biophys. Acta *1365*, 269–277.

Barczuk, P.J., Krolikowska, A., Lewera, A., Miecznikowski, K., Solarska, R., and Augustynski, J. (2013). Structural and photoelectrochemical investigation of boron-modified nanostructured tungsten trioxide films. Electrochem. Acta *104*, 282–288.

Bediako, D.K., Lassalle-Kaiser, B., Surendranath, Y., Yano, J., Yachandra, V.K., and Nocera, D.G. (2012). Structure–Activity correlations in a nickel–borate oxygen evolution catalyst. J. Am. Chem. Soc. *134*, 6801–6809.

Beebo, A., Mathai, J.C., Schoefs, B., and Spetea, C. (2013). Assessment of the requirement for aquaporins in the thylakoid membrane of plant chloroplasts to sustain photosynthetic water oxidation. FEBS Lett. *587*, 2083–2089.

Bennet, J.E. (1980). Electrodes for generation of hydrogen and oxygen from seawater. Int. J. Hydrogen Energy *5*, 401–408.

Bryan, M.H., Harry, B.G., and Astrid, M.M. (2016). Earth-abundant heterogeneous water oxidation catalysts. Chem. Rev. *116*, 14120–14136.

Chemelewski, W.D., Lee, H.-C., Lin, J.-F., Bard, A.J., and Mullins, C.B. (2014). Amorphous FeOOH oxygen evolution reaction catalyst for photoelectrochemical water splitting. J. Am. Chem. Soc. *136*, 2843–2850.

Desilvestro, J., and Gräetzel, M. (1987). Photoelectrochemistry of polycrystalline n-WO_3: electrochemical characterization and photoassisted oxidation process. J. Electroanal. Chem. Interf. Electrochem. *238*, 129–150.

Dionigi, F., Reier, T., Pawolek, Z., Gliech, M., and Stresser, P. (2016). Design criteria, operating conditions, and nickel-iron hydroxide catalyst materials for selective seawater electrolysis. ChemSusChem *9*, 962–972.

El-Moneim, A.A., Kumagai, N., and Hashimoto, K. (2009). Mn-Mo-W oxide anodes for oxygen evolution in seawater electrolysis for hydrogen production. Mater. Trans. *50*, 1969–1977.

Fujimura, K., Izumiya, K., Kawashima, A., Akiyama, E., Habazaki, H., Kumagai, N., and Hashimoto, K. (1999). Anodically deposited manganese-molybdenum oxide anodes with high selectivity for evolving oxygen in electrolysis of seawater. J. Appl. Electrochem. *29*, 765–771.

Fujishima, A., and Honda, K. (1972). Electrochemical photolysis of water at a semiconductor electrode. Nature *238*, 37–38.

Fuku, K., Miyase, Y., Miseki, Y., Gunji, T., and Sayama, K. (2017). WO_3/$BiVO_4$ photoanode coated with mesoporous Al_2O_3 layer for oxidative production of hydrogen peroxide from water with high selectivity. RSC Adv. *7*, 47619–47623.

Fukuzumi, S., Lee, Y.-M., and Nam, W. (2017). Fuel production from seawater and fuel cells using seawater. ChemSusChem *10*, 4264–4276.

Gidon, A., Paz, N., and Youri, G. (2018). Chlorine-free alkaline seawater electrolysis for hydrogen production. Int. J. Hydrogen Energy *43*, 6504–6514.

Hisatomi, T., Kubota, J., and Domen, K. (2014). Recent advances in semiconductors for photocatalytic and photoelectrochemical water splitting. Chem. Soc. Rev. *43*, 7520–7535.

Hong, S.-J., Lee, S., Jang, J.-S., and Lee, J.-S. (2011). Heterojunction $BiVO_4$/WO_3 electrodes for enhanced photoactivity of water oxidation. Energy Environ. Sci. *4*, 1781–1787.

Ibrahim, D., and Canan, A. (2015). Review and evaluation of hydrogen production methods for better sustainability. Int. J. Hydrogen Energy *40*, 11094–11111.

Iguchi, S., Miseki, Y., and Sayama, K. (2018). Efficient hypochlorous acid (HClO) production via photoelectrochemical solar energy conversion using a $BiVO_4$-based photoanode. Sustain. Energy Fuels *2*, 155–162.

Jagendorf, A.T., and Uribe, E. (1966). ATP formation caused by acid-base transition of spinach chloroplasts. Proc. Natl. Acad. Sci. U S A *55*, 170–177.

Kang, D., Kim, T.-W., Kubota, S.-R., Cardiel, A.-C., Cha, H.-G., and Choi, K.-S. (2015). Electrochemical synthesis of photoelectrodes and catalysts for use in solar water splitting. Chem. Rev. *115*, 12839–12887.

Kim, T.W., and Choi, K.-S. (2014). Nanoporous $BiVO_4$ photoanodes with dual-layer oxygen evolution catalysts for solar water splitting. Science *343*, 990–994.

Li, F., Bai, L., Li, H., Wang, Y., Yu, F., and Sun, L. (2016). An iron-based thin film as a highly efficient catalyst for electrochemical water oxidation in a carbonate electrolyte. Chem. Commun. *52*, 5753–5756.

Luo, W., Yang, Z., Li, Z., Zhang, J., Liu, J., Zhao, Z., Wang, Z., Yan, S., Yu, T., and Zou, Z. (2011). Solar hydrogen generation from seawater with a modified $BiVO_4$ photoanode. Energy Environ. Sci. *4*, 4046–4051.

McKenna, S.M., and Davies, K.J. (1988). The inhibition of bacterial growth by hypochlorous acid. Possible role in the bactericidal activity of phagocytes. Biochem. J. *254*, 685–692.

Najafpour, M.M., Ehrenberg, T., Wiechen, M., and Kurz, P. (2010). Calcium manganese(III) oxides ($CaMn_2O_4.xH_2O$) as biomimetic oxygen-evolving catalysts. Angew. Chem. Int. Ed. *49*, 2233–2237.

Raveau, B., and Seikh, M.M. (2012). Cobalt Oxides: From Crystal Chemistry to Physics (*Willey*).

Robinson, S.P., and Downton, W.J.S. (1984). Potassium, sodium, and chloride content of isolated intact chloroplasts in relation to ionic compartmentation in leave. Arch. Biochem. Biophys. *228*, 197–206.

Roger, I., Shipman, M.-A., and Symes, M.-D. (2017). Earth-abundant catalysts for electrochemical and photoelectrochemical water splitting Nat. Rev. Chem. *1*, 0003.

Saito, R., Miseki, Y., and Sayama, K. (2012). Highly efficient photoelectrochemical water splitting using a thin film photoanode of $BiVO_4$/SnO_2/WO_3 multi-composite in a carbonate electrolyte. Chem. Commun. *48*, 3833–3835.

Sauer, K., and Yachandra, V.K. (2002). A possible evolutionary origin for the Mn4 cluster of the photosynthetic water oxidation complex from natural MnO_2 precipitates in the early ocean. Proc. Natl. Acad. Sci. USA *99*, 8631–8636.

Sayama, K. (2018). Production of high-value-added chemicals on oxide semiconductor photoanodes under visible light for solar chemical-conversion processes. ACS Energy Lett. *3*, 1093–1101.

Sivula, K., and van de Krol, R. (2016). Semiconducting materials for photoelectrochemical energy conversion. Nat. Rev. Mater. *1*, 15010–15027.

Suga, M., Akita, F., Sugahara, M., Kubo, M., Nakajima, Y., Nakane, T., Yamashita, K., Umena, Y., Nakabayashi, M., Yamane, T., et al. (2017). Light-induced structural changes and the site of O=O bond formation in PSII caught by XFEL. Nature *543*, 131–135.

Umena, Y., Kawakami, K., Shen, J.-R., and Kamiya, N. (2011). Crystal structure of oxygen-evolving photosystem II at a resolution of 1.9 Å. Nature *473*, 55–60.

Vos, J.G., Wezendonk, T.A., Jeremiasse, A.W., and Koper, M.T.M. (2018). MnOx/IrOx as selective oxygen evolution electrocatalyst in acidic chloride solution. J. Am. Chem. Soc. *140*, 10270–10281.

Yano, J., Kern, J., Sauer, K., Latimer, M.J., Pushkar, Y., Biesiadka, J., Loll, B., Saenger, W., Messinger, J., Zouniand, A., et al. (2006). Where water is oxidized to dioxygen: structure of the photosynthetic Mn_4Ca cluster. Science *314*, 821–825.

Zaharueva, L., Najafpour, M.M., Wiechen, M., Haumann, M., Kurz, P., and Dau, H. (2011). Synthetic manganese–calcium oxides mimic the water-oxidizing complex of photosynthesis functionally and structurally. Energy Environ. Sci. *4*, 2400–2408.

Zhang, B., Daniel, Q., Fan, L., Liu, T., Meng, Q., and Sun, L. (2018). Why nature chose the Mn_4CaO_5 cluster as water-splitting catalyst in photosystem II: a new hypothesis for the mechanism of O–O bond formation. iScience *4*, 144–152.

Zhong, M., Hisatomi, T., Kuang, Y., Zhao, J., Liu, M., Iwase, A., Jia, Q., Nishiyama, H., Minegishi, T., Nakabayashi, M., et al. (2015). Surface modification of CoO_x loaded $BiVO_4$ photoanodes with ultrathin p-type NiO layers for improved solar water oxidation. J. Am. Chem. Soc. *137*, 5053–5060.

iScience, Volume *23*

Supplemental Information

Functions of MnO_x in NaCl Aqueous Solution for Artificial Photosynthesis

Sayuri Okunaka, Yugo Miseki, and Kazuhiro Sayama

Supplemental Information

Table of Contents

Transparent Methods

Materials

Metal organic solutions of Mn, Co, Fe, Ni were purchased from Symetrix Co., USA (purchased from Koujundo Chemical. Co., Japan). $H_2PtCl_6 \cdot 6H_2O$ and $Rh(NO_3)_3$, $IrCl_3$, $AgNO_3$, NaCl, NaH_2PO_4 were purchased from Wako Pure Chemical, Japan. $Pd(NO_3)_2$, RuCl were purchased from Nakalai Tesque. All reagents were used as received, and all the experiments were carried out under ambient condition without eliminating the moisture from the atmosphere.

Preparation of $BiVO_4/WO_3$/FTO photoanode

$BiVO_4/WO_3$/FTO photoanodes were prepared as follows. Precursor solutions of each oxide semiconductor were coated on F-doped SnO_2 conductive glass substrate (FTO; 10 Ω sq^{-1}, Nippon Sheet Glass Co.) by spin-coating and then calcination for each coating. A WO_3 underlayer was coated on the FTO substrate by spin-coating (1500 rpm, 15 s) aqueous peroxo-tungstic acid solution (1.4 M) containing W ions, followed by calcination at 500 °C for 30 min in air. The $BiVO_4$ layer on WO_3/FTO was also fabricated by spin-coating (1000 rpm, 15 s) using a Bi and V precursor solution, followed by calcination at 550 °C for 30 min in air. The $BiVO_4$ precursor solutions was a mixed solution of 0.2 M Bi^{3+} and 0.2 M V^{5+} in a 1:1 volume ratio diluted with butyl acetate.

Preparation of $MO_x/BiVO_4/WO_3$/FTO photoanodes and MO_x/FTO anodes

The MO_x (where M = Mn, Co, Fe, Ni, Pt, Rh) layers on the $BiVO_4/WO_3$/FTO photoanodes (denoted as $MO_x/BiVO_4/WO_3$/FTO) or FTO anodes (denoted as MO_x/FTO) were prepared by spin-coating (1500 rpm, 15 s) metal organic solutions in butyl acetate on the $BiVO_4/WO_3$/FTO and calcination at 400 °C in air for 1 h. In the case of loading the non-noble metals, metal organic solutions (Symetrix Co., USA, purchased from Koujundo Chemical. Co., Japan) in butyl acetate (0.1 M) were used. In the cases of loading with noble metals, aqueous solutions of $H_2PtCl_6 \cdot 6H_2O$ (Wako), $Rh(NO_3)_3$ (Wako) were prepared. It is difficult to prepare high concentration solutions of these noble metal precursor salts; therefore, the concentration of these solutions was adjusted to 0.03 M.

The expression MO_x was used, regardless the valence of the metal. To evaluate the reaction sites, Pt (VD) was coated onto FTO or MnO_x (0.1 M)/FTO by vapor deposition method under vacuum (JFC-1600, JEOL, emission current: 40 mA, emission time: 7 min, sample distance: 30 mm).

For the electrodes used in the electrolysis system under dark conditions, FTO anode electrodes modified with various metal oxides (MO_x/FTO, where M = Mn, Co, Fe, Ni, Cu, Ag, Pt, Pd, Rh, Ru) were prepared. In the case of loading the non-noble metals, metal organic solutions in butyl acetate (0.03 or 0.1 M) were used. In the cases of loading with noble metals, aqueous solutions of $H_2PtCl_6 \cdot 6H_2O$, $Rh(NO_3)_3$, $Pd(NO_3)_2$, RuCl, $AgNO_3$ and $IrCl_3$ were prepared. It is difficult to prepare high concentration solutions of these noble metal precursor salts; therefore, the concentration of these solutions was adjusted to 0.03 M. The MO_x layers on the FTO electrodes (denoted as MO_x/FTO) were prepared by spin-coating (1500 rpm, 15 s) metal organic solutions in butyl acetate on the FTO and calcination at 400 °C in air for 1 h.

To examine the effect of manganese species on FE (HClO), Mn_2O_3/FTO, Mn_3O_4/FTO,

and Ca-MnO_x/FTO anodes were prepared as follows. A Mn_2O_3/FTO anode was prepared by electrochemical deposition (ED-S) in a solution of 0.25 M $MnSO_4$ and 0.25 M Na_2SO_4 (1:1 v/v) for 10 min. The films were rinsed with water and dried, followed by calcination at 400 °C for 1 h in air (Ramírez. et al. 2014). The Mn_3O_4/FTO anode was prepared by electrochemical deposition (ED-N) in a solution of 0.25 M $Mn(NO_3)_2$ and 0.25 M Na_2SO_4 (1:1 v/v) for 10 min at 70 °C. (Qi. et al. 2016) The films were rinsed with water and dried at 80 °C for 1 h in air. A Ca-MnO_x(Mn/Ca=4) anode was prepared by spin-coating (1500 rpm, 15 s) metal organic solutions (0.1 M, Ca:Mn = 1:4 molar ratio, Symetrix Co., USA, purchased from Koujundo Chemical. Co., Japan) in butyl acetate on the FTO and calcination at 400 °C in air for 1 h.

Characterization

The anode samples obtained were characterized using X-ray diffraction (XRD; PANalytical, EMPYREAN, rotating anode diffractometer, 40 kV, 10 mA) with Cu $K\alpha$ radiation ($\lambda_{K\alpha}$ = 1.5406Å), X-ray fluorescence (XRF; Rigaku, Supermini200), X-ray photoelectron spectroscopy (XPS; Ulvac Co., XPS-1800), scanning electron microscopy (SEM; HITACHI, S-4100), and transmission electron microscopy (TEM; Hitachi High-Technologies Co., Ltd., HD2700) with energy dispersive X-ray spectroscopy (EDX) mapping. The MnO_x coverage was calculated using the spectrum area obtained from XPS spectrum and intensity factor of Mn to the sum of those of Mn, Bi, V, W and Sn.

Photoelectrochemical and electrochemical production of HClO and O_2

Photoelectrochemical properties

The photoelectrochemical performance of the photoanodes was measured using an electrochemical analyzer (BAS. Inc., ALS 760E) and a solar simulator (SAN-EI ELECTRIC Co., XES-151S) calibrated to AM-1.5 (1 SUN, 100 mW cm^{-2}) with a spectroradiometer (SOMA Optics, Ltd., Model S-2440). The irradiation area (0.28 cm^2) was defined using a black mask. The simulated solar light was irradiated from the semiconductor side. The current–voltage (*I–V*) characteristics were measured using a two-compartment cell (Pyrex-made) with an ion-exchange membrane (SELEMION, AGC Engineering), and a photoanode equipped with a back-reflection plate as the working electrode, an Ag/AgCl electrode as the reference electrode, and a Pt wire as the counter electrode The scan rate was 50 mV s^{-1}. The measured potentials vs. Ag/AgCl were converted to the standard hydrogen electrode (SHE) and the reversible hydrogen electrode (RHE) scale according to:

$$E_{SHE} = E_{Ag/AgCl} + 0.206 \qquad \text{(S1)}$$

$$E_{RHE} = E_{Ag/AgCl} + 0.059pH + E^{o}{}_{Ag/AgCl} \qquad \text{(S2)}$$

where E_{SHE} and E_{RHE} are the converted potential vs. SHE or RHE, $E^{o}{}_{Ag/AgCl}$ = 0.1976 at 25 °C, and $E_{Ag/AgCl}$ is the experimentally measured potential against the Ag/AgCl reference. An aqueous solution of 0.5 M NaCl (35 mL, pH = 5.9) was used as the electrolyte.

Electrochemical properties

The current–voltage (*I–V*) characteristics on the FTO and MO_x/FTO anodes were measured using a two-compartment cell (Pyrex-made) with an ion-exchange membrane (SELEMION, AGC Engineering), and an anode as the working electrode, an Ag/AgCl electrode as the reference electrode, and a Pt wire as the counter electrode. The scan rate was 50 mV s^{-1}. The measured potentials vs. Ag/AgCl were converted to the SHE and the RHE. An aqueous solution of 0.5 M NaCl (35 mL, pH = 5.9) was used as the electrolyte.

Simultaneous production of HClO and O_2

The simultaneous production of HClO and O_2 on the photoanodes was measured using an electrochemical analyzer (BAS. Inc., ALS 760E) and a solar simulator (SAN-EI ELECTRIC Co., XES-151S) calibrated to AM-1.5 (1 SUN, 100 mW cm^{-2}) with a spectroradiometer (SOMA Optics, Ltd., Model S-2440). The simulated solar light was irradiated from the semiconductor side. The reaction on the obtained photoanodes was performed under solar light irradiation using a two-compartment cell, equipped with an ion-exchange membrane (SELEMION, AGC Engineering) between the anode and cathode. Pt wire was used as a counter electrode to effectively reduce water to H_2. An aqueous solution (anode: 35 mL; cathode: 35 mL) of NaCl (0.5 M) was used as the electrolyte. In the photoelectrochemical reaction, photoanodes (1.5×5 cm) were used. Each solution was stirred by magnetic stirring at ca. 400 rpm. In the case of the FTO and MO_x/FTO anodes, the production of HClO in the dark was conducted by the same method.

The concentration of HClO produced was measured with a UV-vis spectrometer (JASCO, Y-730) using the *N,N*-diethyl-*p*-phenylenediamine (DPD) method. The faradaic efficiencies (FEs) of HClO (FE (HClO)) can be calculated as:

$$FE(HClO) = \frac{(amount\ of\ generated\ HClO)}{(theoretical\ amount\ of\ HClO)} \times 100 = \frac{(amount\ of\ generated\ HClO)}{(amount\ of\ generated\ electrons/2)} \times 100 \quad \text{(S3)}$$

The amount of O_2 evolved in both the liquid and gas phases were determined using an O_2 sensor (Optical Oxygen Meter, Pyro Science and FireStingO_2) and combining each value. These HClO/O_2 production reactions of the main part were measured 3 times, and the reproducibility of the data was confirmed with the variation of experimental errors within 10%. The amount of hydrogen evolved from Pt electrode was determined with a gas chromatograph equipped with a TCD detector. The faradaic efficiency of H_2 (FE (H_2)) can be calculated as:

$$FE(HClO) = \frac{(amount\ of\ generated\ H_2)}{(theoretical\ amount\ of\ H_2)} \times 100 = \frac{(amount\ of\ generated\ H_2)}{(amount\ of\ generated\ electrons/2)} \times 100 \quad \text{(S4)}$$

Results

Table S1. Potential required for photo-electrolysis for steady current (2 mA) using various MO_x/$BiVO_4$/WO_3/FTO photoelectrodes. Related to Figure 2.

MO_x/$BiVO_4$/WO_3/FTO	Potential (V vs. SHE, pH=7)
None	0.74
Mn	0.83
Co	0.68
Ni	0.70
Fe	0.78
Pt	0.65
Rh	0.80

Potential required for electrolysis with an electric charge of 2 C in 0.5 M aqueous NaCl solution using various MO_x/ $BiVO_4$/WO_3/FTO electrodes (1.5 cm x 5 cm). The concentration of loaded metal precursor solution was 0.03 M.

Table S2. Amount of MO_x loading on the $BiVO_4$/WO_3/FTO photoanodes. Related to Figure 2.

MO_x	MO_x loading (μmol/cm^2)
None	0
Mn	0.020
Co	0.014
Fe	0.017
Ni	0.024
Rh	0.016
Pt	0.010

Amount of MO_x loading on the $BiVO_4$/WO_3/FTO photoanodes was calculated using XRF spectra. The concentrations of loaded metal precursor solutions were (a) 0.1 M for Mn, Co, Ni, and Fe, and (b) 0.03 M for Rh and Pt.

Table S3. Apparent MO_x-coverage (%) for the $BiVO_4$/WO_3/FTO photoanodes. Related to Figure 2.

MO_x	Coverage (%)	
	(A) 0.03 M	(B) 0.1 M
Mn	54.0	100.0
Co	51.6	79.9
Ni	77.6	91.9
Fe	79.3	87.4
Rh	32.1	-
Pt	38.5	-

Apparent MO_x-coverage (%) calculated from XPS spectra for $BiVO_4$/WO_3/FTO photoanodes modified with various metal oxides (MO_x). The concentrations of the coated metal precursor solutions were (A) 0.03 M for Mn, Co, Ni, Fe, Rh and Pt, and (B) 0.1 M for Mn, Co, Ni, and Fe. The MnO_x coverage was calculated using the spectrum area and intensity factor of Mn to

the sum of those of Mn, Bi, V, W and Sn.

Table S4. Amounts of adsorbed Cl^- ions on the MO_x/FTO after dipped in NaCl aq. Related to Figure 4.

MO_x	Amount of Cl (%) after immersion in NaCl aq.
None	0.2
Mn	0.2
Co	< 0.1
Ni	0.5
Fe	0.6
Pt	3.2
Rh	3.5

Amounts of adsorbed Cl^- ions on the MO_x/FTO anode after immersion in 10 mL of 0.5 M aqueous NaCl solution for 3 h, determined from XPS measurements. Although the amount of Cl^- adsorption on Pt and RhO_x on the FTO was slightly larger than that of other typical metals, this is because the precursor solutions of Pt and Rh contain Cl^- ions.

Table S5. Potential required for electrolysis for steady current (2 mA) using various MO_x/FTO electrodes. Related to Figure 4.

MO_x/FTO	(A) Potential (V vs. SHE) in NaCl aq.	(B) Potential (V vs. SHE) in NaH_2PO_4 aq.
None	2.43	2.45
Mn	1.62	1.40
Co	1.50	1.38
Ni	1.61	1.50*
Fe	1.67	1.44
Cu	1.95*	2.23*
Cr	1.95*	2.19*
Ag	1.74	1.86
Pt	1.23	1.34
Pd	2.04*	1.50
Rh	1.38	1.37
Ru	1.35	1.36
Ir	1.30	1.36

Potential after the electrolysis with an electric charge of 2 C (1000 s, in a steady current of 2 mA) in (A) 0.5 M aqueous NaCl solution (pH 5.9) and (B) 0.5 M aqueous NaH_2PO_4 solution (pH 4.3) using various MO_x/FTO electrodes (1.5 cm x 4 cm). The concentration of loaded metal precursor solution was 0.03 M. *Elution was observed during the reaction.

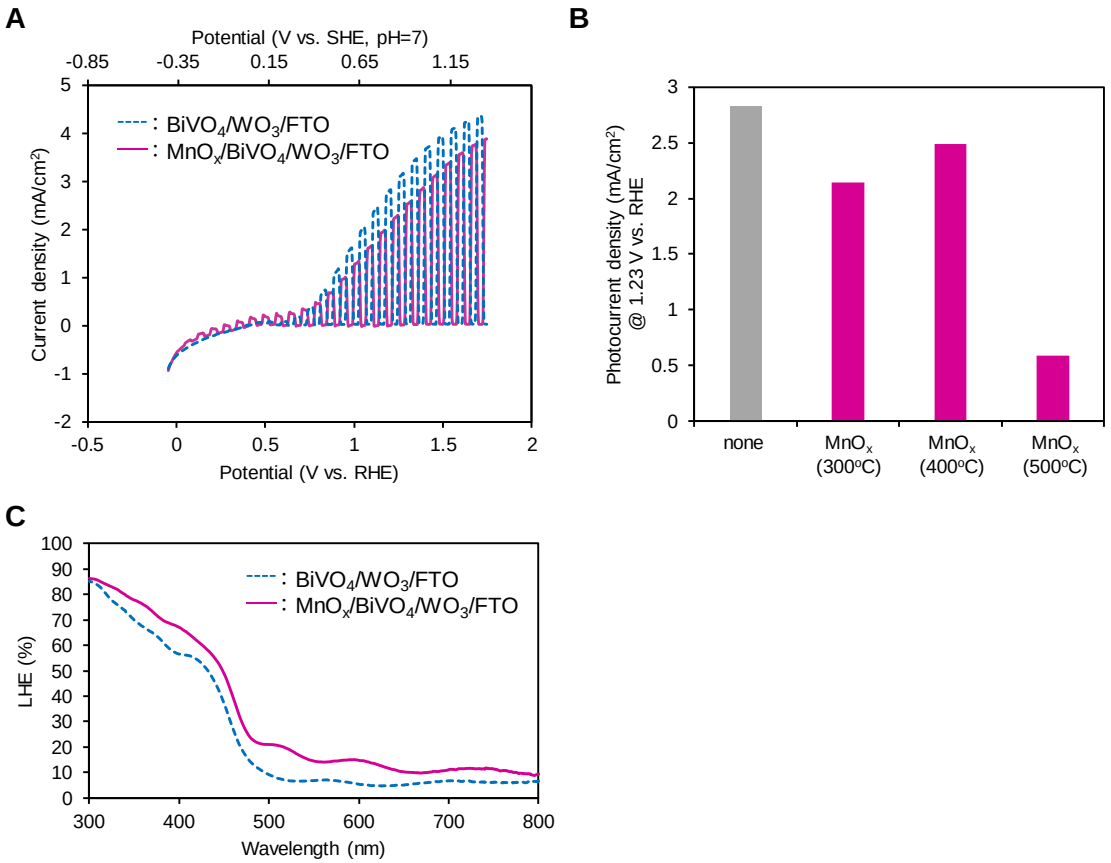

Figure S1. Photoelectrochemical performance and optical property of photoanode. Related to Figure 2.

(A) *I-V* characteristics for bare $BiVO_4/WO_3$/FTO and MnO_x(0.1M)/$BiVO_4/WO_3$/FTO photoanodes measured in 0.5 M NaCl aqueous solution under simulated solar light (AM-1.5, 1 SUN, irradiation area: 0.28 cm^2, irradiated from the semiconductor side) with a light chopper. MnO_x was prepared using 0.1 M-Mn precursor solution and by calcination at 400 °C. (B) Photocurrent at + 0.88 V vs. SHE at pH=7 of the bare $BiVO_4/WO_3$/FTO and MnO_x(0.1M)/$BiVO_4/WO_3$/FTO photoanodes, which were calcined at different temperatures (300 – 500 °C) after coating of the manganese precursor solution, measured in 0.5 M NaCl aqueous solution under simulated solar light. (C) Light harvesting efficiency (LHE) spectra for the bare $BiVO_4/WO_3$/FTO and MnO_x(0.1M)/$BiVO_4/WO_3$/FTO photoanodes calcined at 400 °C after coating with the manganese precursor solution. LHE was calculated from transmittance (T, %) and reflectance (R, %) using the following formula:

$$LHE(\%) = 100 - T - R \qquad \text{(S5)}$$

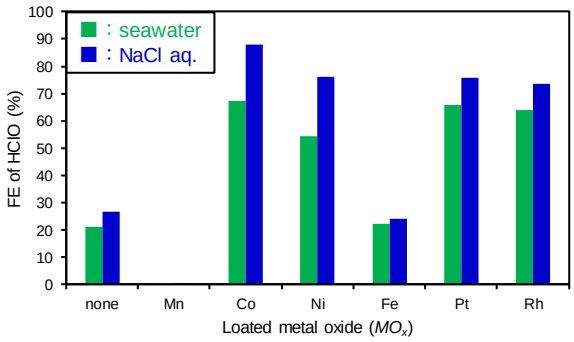

Figure S2. FE(HClO) on photoanodes in 0.5 M of NaCl aq. and artificial seawater. Related to Figure 2.

FEs for oxidative HClO generation on photoanodes (MO_x/$BiVO_4$/WO_3/FTO) modified with and without various metal oxides at an electric charge of 2 C (1000 s at steady photocurrent of 2 mA) in 0.5 M of NaCl aq. and artificial seawater (35 mL) under simulated solar light (AM-1.5, 1 SUN). The concentrations of coated metal precursor solutions were 0.1 M for Mn, Co, Ni, and Fe, and 0.03 M for Rh and Pt. The artificial seawater (MARINE ART SF-1) was purchased from Osaka Yakken. Co. Ltd., Japan (Iguchi. et al. 2018).

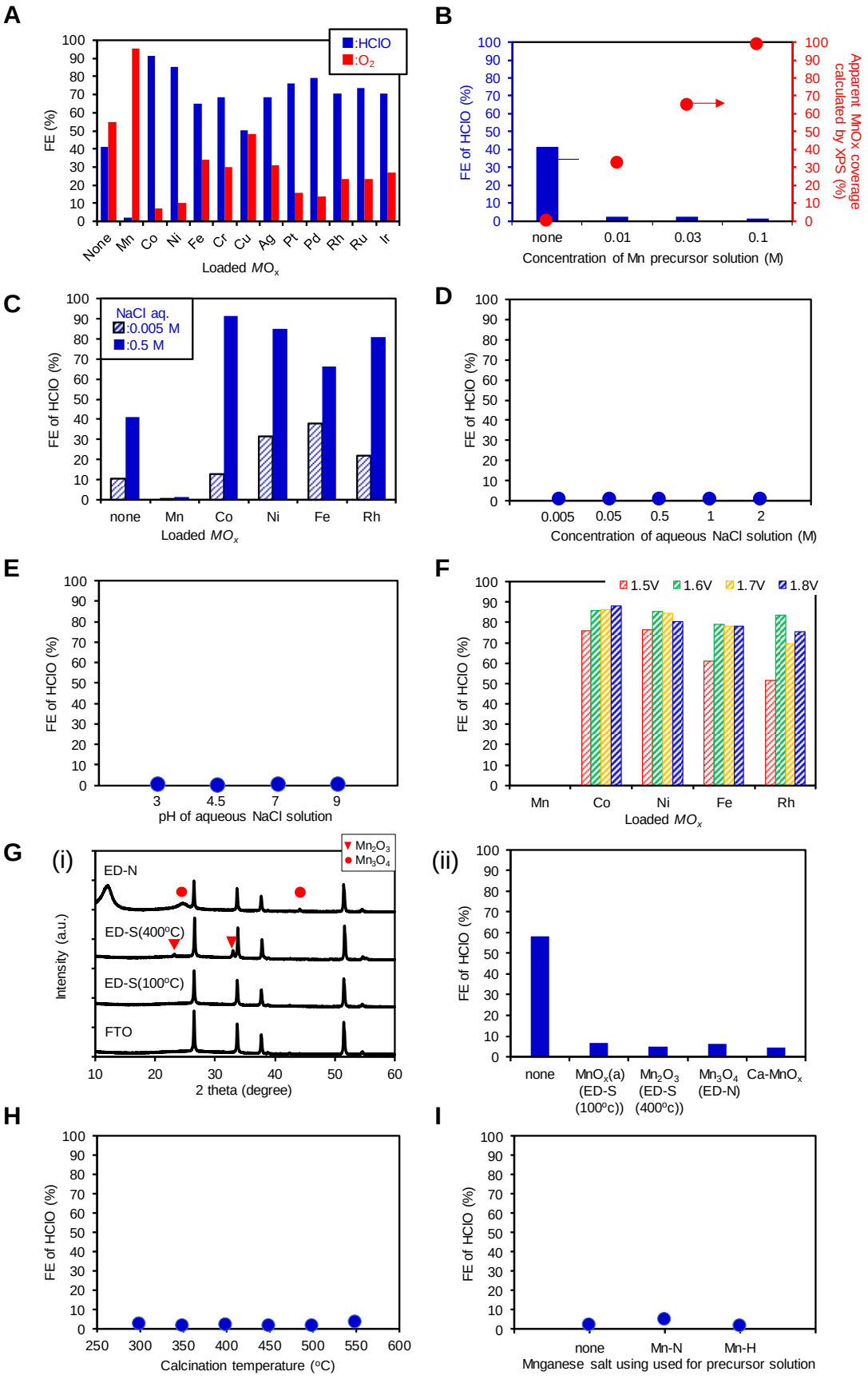
A
FE (%)
:HClO
:O2
None Mn Co Ni Fe Cr Cu Ag Pt Pd Rh Ru Ir
Loaded MOx
B
FE of HClO (%)
Apparent MnOx coverage calculated by XPS (%)
none 0.01 0.03 0.1
Concentration of Mn precursor solution (M)
C
FE of HClO (%)
NaCl aq.
:0.005 M
:0.5 M
none Mn Co Ni Fe Rh
Loaded MOx
D
FE of HClO (%)
0.005 0.05 0.5 1 2
Concentration of aqueous NaCl solution (M)
E
FE of HClO (%)
3 4.5 7 9
pH of aqueous NaCl solution
F
FE of HClO (%)
1.5V 1.6V 1.7V 1.8V
Mn Co Ni Fe Rh
Loaded MOx
G
(i)
Mn2O3
Mn3O4
ED-N
ED-S(400°C)
ED-S(100°C)
FTO
Intensity (a.u.)
2 theta (degree)
(ii)
FE of HClO (%)
none
MnOx(a) (ED-S (100°c))
Mn2O3 (ED-S (400°c))
Mn3O4 (ED-N)
Ca-MnOx
H
FE of HClO (%)
250 300 350 400 450 500 550 600
Calcination temperature (°C)
I
FE of HClO (%)
none Mn-N Mn-H
Mnganese salt using used for precursor solution

Figure S3. FEs for HClO generation on MO_x/FTO under dark conditions. Related to Figure 2.

The electric charge was 2 C (1000 s at a steady photocurrent of 2 mA) under various conditions. (A) FE (HClO) and FE(O_2) on MO_x (0.03 M)/FTO in 0.5 M aqueous NaCl solution. (B) FE (HClO) and apparent MnO_x-coverage calculated from XPS results for bare FTO and MnO_x/FTO photoanodes, which were prepared by coating the manganese precursor solution with different concentrations (0.01–0.1 M) to change the MnO_x loading amount. (C) FE (HClO) on bare FTO and MO_x/FTO in 0.005 M or 0.5 M aqueous NaCl solution. (D) FE (HClO) on MnO_x (0.1 M)/FTO in aqueous NaCl solution with various concentrations (0.005–2 M). (E) FE (HClO) on MnO_x (0.1 M)/FTO anode in 0.5 M aqueous NaCl solution with various pH (pH 3–9). (F) FE (HClO) on various MO_x/FTO anode at steady potentials (1.5–1.8 V vs. SHE, pH=7) in 0.5 M aqueous NaCl solution. pH was adjusted by using NaOH and HCl. For the MO_x/FTO electrodes (1.5 cm x 4 cm) used in the experiments of (B), (C) and (D), the concentrations of the coated metal precursor solution were 0.1 M for Mn, Co, Ni, and Fe, and 0.03 M for Rh. (G-i) XRD patterns of the various MnO_x/FTO anodes prepared by electrochemical deposition and followed by calcination at various temperatures. In the XRD pattern of MnO_x(ED-S(100°C)/FTO anode, no diffraction peak originated from the coating metal oxide, indicative of their amorphicity. (G-ii) FE (HClO) for MnO_x/FTO anodes prepared by electrochemical deposition followed by calcination at various temperatures, and that for the Ca-MnO_x anode in a 0.5 M aqueous NaCl solution. (H) FE (HClO) on MnO_x/FTO electrodes prepared by changing different calcination temperatures (300-550°C) in 0.5 M aqueous NaCl solution. (I) FE (HClO) on MnO_x/FTO electrodes prepared by using different manganese precursor salt ($Mn(NO_3)_2$•$6H_2O$ and manganese bis(2-ethylhexanoate)) The obtained electrodes are denoted that Mn-N, Mn-H, respectively.

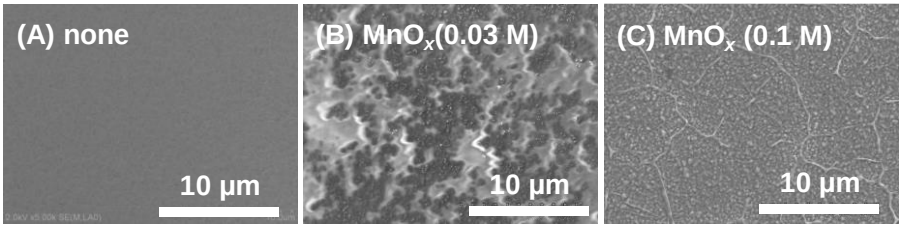

Apparent MnO_x coverage	0%	65%	99%
FE(HClO)	41.3%	< 2.4%	< 1.6%

Figure S4. SEM images and MnO_x coverages of (A) FTO substrate and (B)(C) MnO_x/FTO anodes. Related to Figure 3.

Manganese precursor solutions with different concentrations ((B) 0.03 M and (C) 0.1 M) were spin-coated on FTO, and calcined at 400 °C. The apparent MnO_x coverage was evaluated by using XPS spectra of Mn 2p to Sn 3d and these counts per seconds (cps) coefficients.

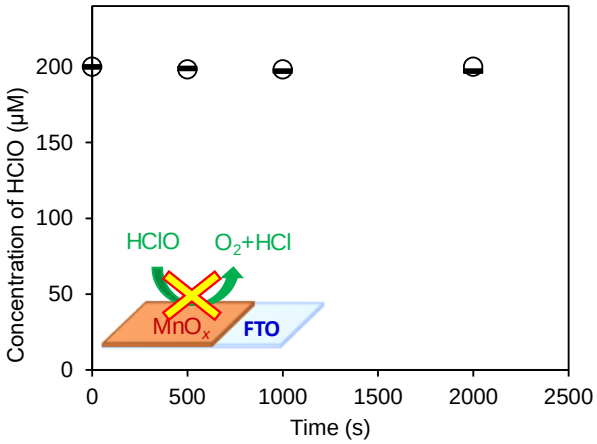

Figure S5. HClO degradation behavior for MnO_x (0.1 M)/FTO under dark conditions. Related to Figure 4, 5.

HClO degradation reactions were performed by using MnO_x (0.1 M)/FTO under dark conditions in 0.5 M aqueous NaCl solution (35 mL) with initial addition of 200 μM of NaClO; (i) without current flow (-), and (ii) at a steady current of 2 mA (○).

References:

Ramírez, A. et al. (2014) Evaluation of MnO_x, Mn_2O_3, and Mn_3O_4 Electrodeposited Films for the Oxygen Evolution Reaction of Water. *J. Phys. Chem. C 118*, 14073−14081.

Qi, Z., Younis, A., Chu, D., Li, S. (2016) A Facile and Template-Free One-Pot Synthesis of Mn_3O_4 Nanostructures as Electrochemical Supercapacitors. *Nano-Micro Lett. 8*, 165–173.

Iguchi, S., Miseki Y., Sayama, K. (2018) Efficient Hypochlorous Acid (HClO) Production *via* Photoelectrochemical Solar Energy Conversion Using a $BiVO_4$-based photoanode. *Sustainable Energy Fuels 2*, 155–162.